

Research Article

Interaction model estimation-based robotic force-position coordinated optimization for rigid–soft heterogeneous contact tasks

Haochen Zheng^{a,b}, Xueqian Zhai^a, Hongmin Wu^{a,*}, Jia Pan^c, Zhihao Xu^a, Xuefeng Zhou^a^a Institute of Intelligent Manufacturing, Guangdong Academy of Sciences, Guangdong Key Laboratory of Modern Control Technology, Guangzhou 510070, China^b School of Rail Transportation, Wuyi University, Jiangmen 529020, China^c Department of Computer Science, The University of Hong Kong, Hong Kong 999077, China

ARTICLE INFO

Article history:

Received 28 September 2024

Revised 23 October 2024

Accepted 3 November 2024

Available online 19 November 2024

Keywords:

Heterogeneous contact

Interaction model estimation

Coordination optimization

Model Predictive Control

ABSTRACT

Inspired by Model Predictive Interaction Control (MPIC), this paper proposes differential models for estimating contact geometric parameters and normal-friction forces and formulates an optimal control problem with multiple constraints to allow robots to perform rigid–soft heterogeneous contact tasks. Within the MPIC, robot dynamics are linearized, and Extended Kalman Filters are used for the online estimation of geometry-aware parameters. Meanwhile, a geometry-aware Hertz contact model is introduced for the online estimation of contact forces. We then implement the force-position coordinate optimization by incorporating the contact parameters and interaction force constraints into a gradient-based optimization MPC. Experimental validations were designed for two contact modes: “single-point contact” and “continuous contact”, involving materials with four different Young’s moduli and tested in human arm “relaxation–contraction” task. Results indicate that our framework ensures consistent geometry-aware parameter estimation and maintains reliable force interaction to guarantee safety. Our method reduces the maximum impact force by 50% and decreases the average force error by 42%. The proposed framework has potential applications in medical and industrial tasks involving the manipulation of rigid, soft, and deformable objects.

© 2024 The Author(s). Published by Elsevier B.V. on behalf of Shandong University. This is an open access article under the CC BY-NC-ND license (<http://creativecommons.org/licenses/by-nc-nd/4.0/>).

1. Introduction

Human adaptability in heterogeneous contact manipulation tasks includes proficiency in handling objects of various shapes, such as rigid, deformable, and soft, thanks to ontological perception of geometric parameters and contact dynamics. However, robots face major challenges in this scenario. Traditional robot control methods are difficult to show human-like adaptability in heterogeneous contact tasks, especially in tasks that require strong perception of contact objects. During medical tasks (e.g., palpation [1], ultrasound testing [2], surgery of surface tissues [3]), because the different tissues and organs of the human body show the characteristics of rigidity and flexibility, the contact characteristics of the contact process are changed between rigidity and flexibility. In industrial tasks (for example, laying carbon fiber sheet [4] on a thin-walled part, drilling a heterogeneous structure [5]), the workpiece itself has rigid characteristics, but in the process of contact processing tasks will occur a certain degree of flexible deformation. Thus, it has heterogeneous contact characteristics (see Fig. 1).

The widespread application of robots in medical and industrial fields exacerbates these challenges. Extensive research has addressed rigid and compliant contact issues using methods such as reinforcement learning-based approaches [6], quadratic programming [7] or model predictive control [8]. Unlike rigid contact, flexible contact depends on material properties and deformation factors, which can be addressed through methods resembling human skill demonstrations [9,10] or tactile perception [11]. Compared to these two types of contact tasks, heterogeneous contact tasks pose distinctive challenges, primarily due to:

- Diverse surface characteristics in heterogeneous contacts, the high computational complexity of multi-degree-of-freedom robot dynamics models, and a lack of real-time physical perception for online estimation of contact parameters such as contact normals, points, and stiffness;
- Discontinuous dynamics in heterogeneous contacts, lacking adaptive interactive contact dynamic models;
- Potential for large impact forces and non-contact bouncing during cross-material operations, necessitating coordinated optimization of contact locations and interaction forces.

To address these challenges, inspired by the Model Predictive Interaction Control (MPIC) scheme [12,13], we propose a

* Corresponding author.

E-mail address: hongminwu0120@gmail.com (H. Wu).

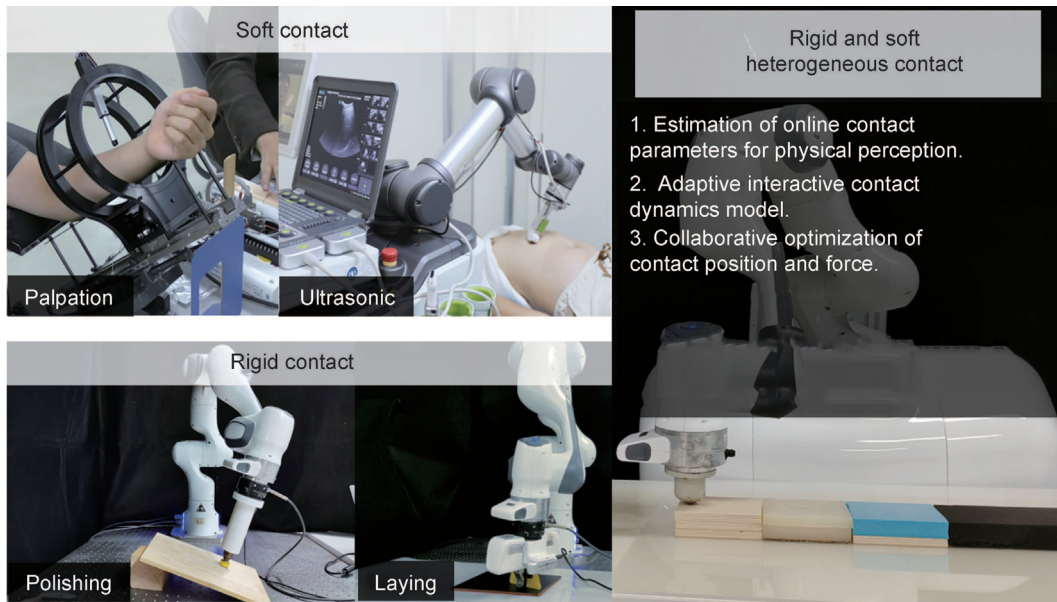


Fig. 1. The robot is in contact with the environment, involving objects with different physical characteristics such as rigid, deformable, and soft, etc. The traditional robot control scheme with fixed control parameters cannot be adapted to the heterogeneous contact tasks.

framework of interaction model estimation-based robotic force-position coordinated optimization for rigid–soft heterogeneous contact tasks, in which we attempt to use the differential models for estimating contact geometric parameters and interactive normal-friction forces to construct a multi-constraint optimization optimal control problem (OCP) [14,15], capable of handling both rigid and soft contact scenarios. The primary contributions are as follows:

- (1) Estimation of geometry-aware contact parameters: Considering the complexity and discontinuity of contact dynamics, the robot dynamics are initially linearized to simplify the contact model. Extended Kalman filtering is then used to estimate the geometry-aware parameters of the contact surface during the interaction;
- (2) Estimation of contact forces: Integrated the geometry-aware Hertz contact model into the model predictive interaction control strategy, as such the model enables online estimation of contact normal and friction forces during fixed or continuous contact interactions;
- (3) Collaborative optimization of force and position hybrid control: Integrating contact parameters and interaction force constraints into gradient-based optimization MPC, achieving force-position collaborative optimization.

This enables robots to perform rigid–soft heterogeneous contact tasks, ensuring stable force control and trajectory tracking during interactions.

2. Related work

In recent years, manipulation tasks involving rigid–soft heterogeneous contacts have gained increasing attention. Magrini et al. [30] addressed contact tasks by dynamically decoupling complementary quantities and utilizing residual methods and external sensors for online estimation of contact points. Huang et al. [36] established a control framework based on generalized fuzzy neural networks to solve model-free soft-touch problems, enabling tracking of required contact states during interactions with the environment. Pang [38] formulated quasi-static dynamics as Karush–Kuhn–Tucker (KKT) optimality conditions for convex Quadratic Programming, predicting motion and forces of

quasi-static systems through QP solving. Cui et al. [40] proposed a model-free Deep Reinforcement Learning (DRL) method integrating force control with independent motion control, achieving precise operations at a single contact point.

These approaches estimate contact states to reduce environmental disturbances during contact processes, thereby enhancing system robustness [42]. Contact dynamics in tasks involving rigid–soft heterogeneous contacts are complex and discontinuous [43], largely influenced by the environment itself [44], with these methods overlooking contact stiffness during interaction with the environment.

To address these challenges, we propose an Extended Kalman Filter (EKF) based on linearized dynamics. Linearizing contact dynamics reduces the complexity of system parameters, thereby enhancing the EKF's capability to estimate contact positions and stiffness online. This method aims to improve system robustness by better incorporating the physical properties of the environment and addressing the complexity of contact dynamics in rigid–soft heterogeneous tasks.

In tasks requiring precise operations in fields like medicine and industry, stable control of contact forces is essential. Wang et al. [28] modeled contact forces using Dynamic Movement Primitives (DMP) based on human skill demonstrations, integrating force DMP modeling with motion DMP modeling in force/motion controllers to estimate contact forces. Gold et al. [16] addressed environmental diversity by constraining kinematics and forces using Model Predictive Control (MPC), achieving contact force estimation in dynamic interaction scenarios. Fu et al. [31] tackled issues in dynamic medical contact tasks by tracking normal contact forces using Quadratic Programming (QP) and ensuring the passivity of optimized systems through energy tanks. Liu et al. [34] combined robot skill learning methods with robot–environment contact states for contact state modeling and force estimation.

These methods consider the diversity and dynamics of robot interaction scenarios, modeling interactive motion and force to reduce disturbances from the contact environment. In tasks involving rigid–soft heterogeneous contacts, contact processes are discontinuous, and friction forces arise during interaction. There-

Table 1

Illustrate the state-of-the-art robot skill learning and optimal control methods during rigid-soft heterogeneous contact tasks.

Index	Materials	Geometry-aware estimation			Force estimation		Method	Optimal control	RW.
		C. Pos.	C. Nor.	C. Kin.	Nor. F.	Fri. F.			
1	Rigid	✓	✓	✓	✓	-	-	MPC	[16–18]
2	Rigid	✓	-	-	✓	-	QP	Impact-aware	[19–21]
3	Simul.	-	✓	✓	✓	✓	QP	MPC	[22–24]
4	Rigid	✓	✓	✓	✓	-	DDPG	Variable gain PD	[25,26]
5	R2R.	✓	✓	-	✓	-	C^∞	Force/Motion	[27]
6	Rigid	-	✓	-	✓	-	-	Force/Motion	[28–30]
7	R2S	✓	✓	✓	✓	-	QP	Impedance	[31–33]
8	Soft	-	✓	✓	✓	-	-	Admittance	[34,35]
9	Soft	-	✓	✓	✓	-	BFNN	Impedance	[36,37]
10	Simul.	-	✓	✓	✓	✓	QP	Impedance	[38,39]
11	Rigid	-	✓	✓	✓	-	-	Force/Motion	[40,40,41]

Note: To the best of our knowledge, this table is an incomplete summary of each kind of approach.

fore, introducing a Hertz contact model with physical awareness into Model Predictive Control strategies for interaction control effectively estimates contact forces while avoiding significant impact forces during contact processes.

In optimizing traditional robot control methods, Wang et al. [19] proposed an impact-aware controller by establishing a viscoelastic contact force model to reduce rigid robot impact forces. Sombolstan et al. [22] introduced a Hierarchical Model Predictive Control approach using QP optimization to satisfy contact constraints, achieving decentralized control for estimating contact information such as contact positions, normal forces, and friction forces. Bogdanovic et al. [25] presented a Deep Deterministic Policy Gradient (DDPG) with a variable-gain PD control method, demonstrating robustness and stability in contact tasks in unknown environments. Aydinoglu et al. [21] proposed a feedback control strategy incorporating both state and tactile feedback for contact tasks under incomplete state information.

The above-mentioned methods improve and optimize traditional control approaches to achieve stability in both motion control and force control aspects. The above methods are summarized in Table 1. Considering the characteristics of tasks involving rigid-soft heterogeneous contacts, such as discontinuous contact objects and complex contact dynamics, there is a need for multi-objective optimization. A force-position coordinated optimization control strategy based on Model Predictive Control is proposed. This strategy aims to effectively manage the inherent complexity and uncertainty in heterogeneous contact tasks, ensuring robust performance in controlling contact forces and achieving precise trajectory tracking.

3. Geometry-aware parameters and contact force estimation during heterogeneous contact

This section mainly introduces three components of the proposed method: Parameter Estimation of Heterogeneous Contact, Force Estimation of Heterogeneous Contact, and MPC-based Hybrid Force-Position Control. The overall framework of the method is illustrated in Fig. 2.

3.1. Geometry-aware parameters estimation during heterogeneous contact

3.1.1. Linearization of robot dynamics

In the context of rigid-soft heterogeneous contact tasks, considering the complexity of contact dynamics, the robot dynamics are linearized. Traditional explicit integration methods for solving rigid differential equations are limited by time step constraints; therefore, a semi-implicit integration method is employed to linearize dynamics. The robot dynamics can be expressed as

$$\begin{bmatrix} q_+ \\ \dot{q}_+ \end{bmatrix} = f \left(\begin{bmatrix} q \\ \dot{q} \end{bmatrix}, \tau, K \right) \quad (1)$$

The joint position and joint velocity at the next time step of length h can be expressed as

$$q_+ = q + h\dot{q}_+ \quad (2)$$

$$\dot{q}_+ = \dot{q} + hM^{-1}(\tau - \delta\sqrt{K}\dot{q}) \quad (3)$$

$$\vartheta = M^{-1}(\tau - \delta\sqrt{K}\dot{q}) \quad (4)$$

where h represents the time step, $q \in \mathbb{R}^n$, ϑ denotes the impulse caused by torque τ , inertia matrix M , and contact stiffness K , δ is the stiffness coefficient. To facilitate estimation of the robot system's state, the state vector of the robot system is represented as $X = [q, \dot{q}, K]$. The robot dynamics equation in terms of the state vector can be linearly approximated as follows:

$$X_+ \approx \begin{bmatrix} I + h^2 \Gamma_q^\vartheta & hI & h^2 \Gamma_K^\vartheta \\ h\Gamma_q^\vartheta & I & h\Gamma_K^\vartheta \\ 0 & 0 & I \end{bmatrix} X + B \quad (5)$$

$$\approx AX + B$$

Γ_x^ϑ denotes the Jacobian of y with respect to x . $\Gamma_q^\vartheta \in \mathbb{R}^{n \times n}$, $\Gamma_K^\vartheta \in \mathbb{R}^{n \times 3}$, $I \in \mathbb{R}^{n \times 3}$ denotes the identity matrix, B represents the bias term.

3.1.2. Interactive stiffness estimation using extended Kalman filter

The state vector at time t can be represented as $X_t^T = [q_t^T, \dot{q}_t^T, K_t^T]$. A method based on linearized dynamics Extended Kalman Filter (EKF) is proposed to estimate the state vector. Linearizing the dynamics equations helps reduce the complexity of system parameters, thereby enhancing the online parameter estimation capability of the filter. The filter estimates the state vector using measurements, which include the robot's joint position q and joint torques τ . The observation vector is represented as $O_t^m = [q_t^m; \tau_t^m]$. The posterior belief about the state vector is represented as

$$P(X_t | O_t^m) = N(\mu_t, \Sigma_t) \quad (6)$$

At any given time, observed joint position q^m and observed torque τ^m can be expressed in terms of the state vector at the same time as follows:

$$\begin{aligned} q^m &= H_q X + \omega_q \\ \tau^m &= H_\tau X + \omega_\tau \end{aligned} \quad (7)$$

For two different observation values, the observation model matrices are represented as $H_q = [I_n, 0_n, 0_3]$, $H_\tau = [\Gamma_q^\tau, 0_n, 0_3]$. The combined observation matrix is $H = [H_q; H_\tau]$. The noise $\omega = [\omega_q; \omega_\tau]$ is independently and identically distributed, where Λ_q and Λ_τ are the observation noise covariance matrices corresponding to joint position and joint torque observations, respectively. $\Lambda = \text{diag}(\Lambda_q, \Lambda_\tau)$, I_n denotes an n -dimensional identity matrix, and 0_n represents an n -dimensional column vector of

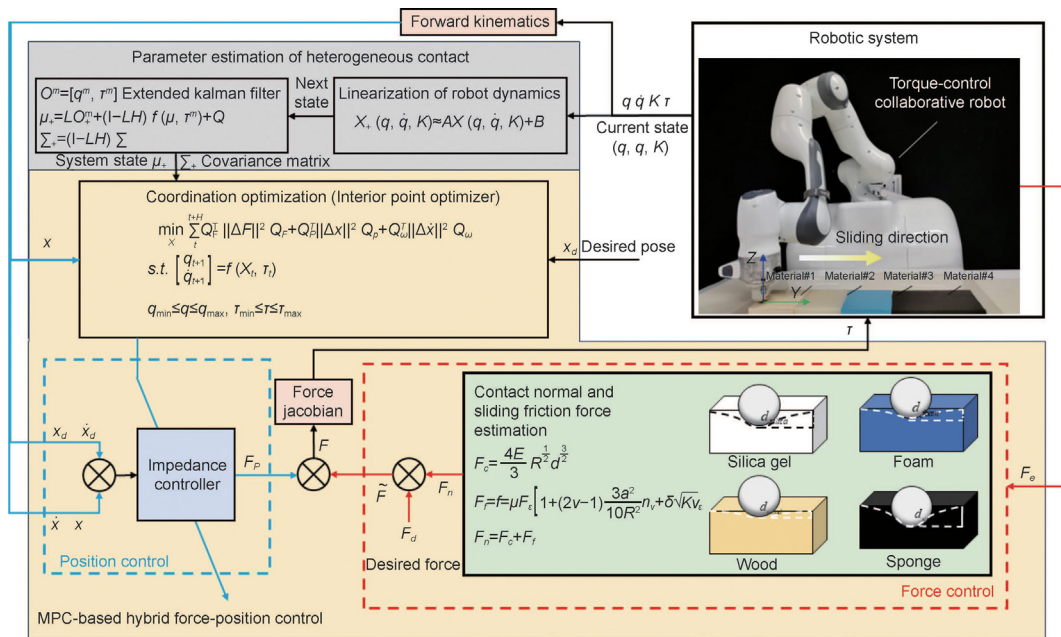


Fig. 2. The framework of the method is divided into three parts: parameter estimation of heterogeneous contact, force estimation of heterogeneous contact, and force-position control based on model predictive control. Parameter estimation obtains the contact position and contact stiffness, force estimation obtains the contact, and the force-position control based on model predictive control is introduced to realize the control of the robot.

zeros. The observation $O_+^m = HX + \omega$. Consequently, after the next time step, the update process for the estimated mean μ_+ and covariance matrix Σ_+ of the state vector can be expressed as:

$$\begin{aligned}
 L &= \Sigma H^T (H \Sigma H^T + \Lambda)^{-1} \\
 \mu_+ &= LO_+^m + (I - LH)f(\mu, \tau^m) + Q \\
 \Sigma_+ &= (I - LH)\Sigma
 \end{aligned}
 \tag{8}$$

Here, L is the Kalman gain, and Q represents process noise. From Eq. (8), the force in Cartesian space generated by position error through the impedance control model can be expressed as:

$$\begin{aligned}
 M\ddot{\tilde{x}} + K_+\tilde{x} + \delta\sqrt{K_+}\dot{\tilde{x}} &= F_p \\
 \tilde{x} &= x_+ - x
 \end{aligned}
 \tag{9}$$

Here $x \in \mathbb{R}^m$, $\dot{x} \in \mathbb{R}^m$, $\ddot{x} \in \mathbb{R}^m$, represent the position, velocity, and acceleration of the end effector of the robot system:

$$\begin{aligned}
 x &= J(q)q \\
 \dot{x} &= J(q)\dot{q} \\
 \ddot{x} &= J(q)\ddot{q} + \dot{J}(q)\dot{q}
 \end{aligned}
 \tag{10}$$

Where $J(q)$ is the Jacobian matrix, q_+ denotes the next time step joint position estimated from the mean state vector, $x_+ = J(q)q_+$ represents the estimated position in Cartesian space at the next time derived from the joint position at the next time. $x \in \mathbb{R}^m$ represents the actual end position of the robot in Cartesian space. In the equations above, $\tilde{x} \in \mathbb{R}^m$, $\dot{\tilde{x}} \in \mathbb{R}^m$, $\ddot{\tilde{x}} \in \mathbb{R}^m$ respectively denote the positional, velocity, and acceleration errors in Cartesian space. The terms M, K_+ correspond to inertia and the estimated contact stiffness at the next time obtained from the estimated mean μ_+ of the state vector.

3.2. Contact force estimation during heterogeneous contact

To better mitigate abrupt changes in force during contact tasks and ensure the stability of force during task execution, this paper models the interaction dynamics between the end effector

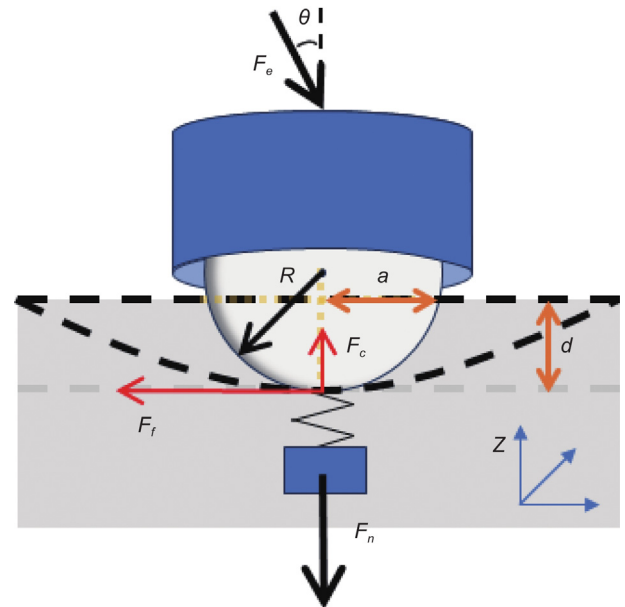


Fig. 3. Schematic diagram of contact normal force, friction force and resultant force under different material contact states.

applied on a robotic arm and the contacted object. During contact interaction, the contact force estimation model is divided into two parts: normal force prediction and tangential force prediction. The contact model between the end of the robot and the contact object is shown in Fig. 3.

3.2.1. Contact normal force

In rigid-flexible heterogeneous contact tasks, where the Young's modulus of the rigid robot is significantly greater than that of the heterogeneous contact object, according to Hertz theory, the approximate Young's modulus E is given by $E = E_2 / (1 - \nu_2^2)$, Where E_2 and ν_2 are Young's modulus and Poisson's ratio of the contact object respectively. The relationship

between deformation force F_c and maximum static deformation d is expressed as

$$F_c = \frac{4E}{3} R^{\frac{1}{2}} d^{\frac{3}{2}} \quad (11)$$

Thus, the normal contact force is $F_n = F_e - F_c \cos \theta$, where θ is the angle between the contact force and the normal to the contact surface, F_e is force imparted on the surface.

3.2.2. Contact friction force

The applied average force F_m on the contact surface is $F_m = \frac{F}{\pi a^2}$, with $a^2 = Rd$, where a is the radius of the contact area. When $r \leq a$:

- Radial force distribution $\sigma_z : \frac{\sigma_z}{F_m} = -\frac{3}{2} \left(1 - \frac{r^2}{a^2}\right)^{\frac{1}{2}}$
- Axial force distribution $\sigma_r : \frac{\sigma_r}{F_m} = \frac{2v-1}{2} \frac{a^2}{r^2} \left[1 + \frac{2}{3} \frac{\sigma_z}{F_m}\right] + 2v \frac{\sigma_z}{F_m}$
- Circumferential force distribution $\sigma_\theta : \sigma_\theta = (2 + v)\sigma_z - \sigma_r$

To obtain frictional stress, the principal stresses on the contact surface are denoted by σ . According to Cauchy stress theory, the principal stress σ in cylindrical coordinates is

$$\sigma = \begin{bmatrix} \sigma_r & 0 & \sigma_{rr} \\ 0 & \sigma_\theta & 0 \\ \sigma_r & 0 & \sigma_z \end{bmatrix} \quad (12)$$

At any point on the contact surface (x, y, z) , the normal vector from this point to the centroid of the robot's end effector sphere is given by $N = [\sin \theta; 0; \cos \theta]$. The normal stress in Cartesian coordinates is obtained as $\sigma_n = N^T T^T \sigma T N$, where T is the transformation matrix. According to the Coulomb friction model, the relationship between the overall frictional force F_f on the contact surface, normal stress σ_n , and area S is $F_f = \mu \sigma_n S$, where μ represents the coefficient of friction. Thus,

$$F_f = f = \mu F_n \left[1 + (2v - 1) \frac{3a^2}{10R^2}\right] n_v + \delta \sqrt{K} v_e \quad (13)$$

Here, δ is the contact stiffness coefficient, K is the contact stiffness, and v_e represents the horizontal velocity on the contact surface, v is the Poisson's ratio of the contact object.

3.3. MPC-based hybrid force-position control

In the context of rigid-flexible heterogeneous contact tasks, traditional control methods struggle to achieve stable tracking of both force and motion. This paper proposes a force-position hybrid control strategy based on Model Predictive Control (MPC). Assuming an n -joint serial robotic arm, the robot's dynamic equations in joint space can be represented as

$$M(q)\ddot{q} + C(q, \dot{q})\dot{q} + G(q) + J(q)^T F_p + J(q)^T \tilde{F} = \tau \quad (14)$$

Here q, \dot{q}, \ddot{q} , denote the position, velocity, and acceleration of the robot joints, respectively. $M(\ddot{q}) \in \mathbb{R}^{n \times n}$, $C(q, \dot{q}) \in \mathbb{R}^{n \times n}$, $G(q) \in \mathbb{R}^n$ represent the inertia matrix, centrifugal and Coriolis forces, and gravitational effects. τ represents the joint torque, F_p denotes the force based on different contact stiffness and position errors, and \tilde{F} represents the feedback force obtained from real-time normal and frictional forces on contact. $\tilde{F} = F_d - (F_c + F_f)$ is obtained from the Eqs. (11), (13). Model Predictive Control (MPC) is an iterative solution based on dynamic optimization problems, capable of simultaneously optimizing multiple process variables. It possesses excellent characteristics such as robustness, flexibility, and real-time capabilities. The entire control framework is implemented using the CasADi¹ library, known for its advanced

algorithmic capabilities and efficient solving speeds. Finally, MPC optimization is achieved through IPOPT [45], which has sophisticated constraint-solving capabilities. The MPC problem is written with the dynamics of Eq. (14),

$$\begin{aligned} \min_x \quad & \sum_t^{t+h} Q_f^T \|\Delta F\|^2 Q_f + Q_p^T \|\Delta x\|^2 Q_p + Q_\omega^T \|\Delta \dot{x}\|^2 Q_\omega \\ \text{s.t.} \quad & \begin{bmatrix} q_{t+1} \\ \dot{q}_{t+1} \end{bmatrix} = f(X_t, \tau_t) \\ & g(X_t, \tau_t) \leq 0 \\ & q_{\min} \leq q \leq q_{\max}; \dot{q}_{\min} \leq \dot{q} \leq \dot{q}_{\max}; \tau_{\min} \leq \tau \leq \tau_{\max} \end{aligned} \quad (15)$$

In the formula, ΔF represents the force error, Δx represents the position error, and $\Delta \dot{x}$ represents the velocity error. Q_f , Q_p , and Q_ω represent the weight matrix of force, position, and velocity, respectively, h represents the time step, and $g(X_t, \tau_t)$ represents the constraint function.

3.3.1. Cost function design

This paper utilizes Model Predictive Control to achieve synergistic optimization of force and position. Force and motion are treated as control objectives in MPC, where the cost Eq. (15) comprises three components: force, position, and velocity.

- $\|\Delta F\|^2 = \left\|F_d - F_p - \tilde{F}\right\|^2$ This term represents the error between the desired force F_d and the actual force $F_p + \tilde{F}$ implemented by the end effector in Cartesian space;
- $\|\Delta x\|^2 = \|x_d - x\|^2$ This term represents the error between the desired position x_d and x the actual position of the end effector in Cartesian space;
- $\|\Delta \dot{x}\|^2 = \|\dot{x}_d - \dot{x}\|^2$ This term represents the error between the desired velocity \dot{x}_d and \dot{x} the actual velocity of the end effector in Cartesian space.

3.3.2. System constraints

During the interaction between the robot and its environment, MPC is used to coordinate the position and force of the entire system through desired constraints. The overall constraint strategy is formulated as

$$g(X_t, \tau_t) = F_{\max} - K_t (J(q)q_t - x_d) - \delta \sqrt{K_t} (J(q)\dot{q}_t) - J(q)^T \tau_t \leq 0 \quad (16)$$

The constraint function g regulates the robot's effective position and force via the impedance control model, thereby preventing the robot from moving outside the designated workspace and avoiding the generation of excessive forces, where F_{\max} is the maximum permissible force, δ is the contact stiffness coefficient, K is the contact stiffness, X_t denotes the state vector at time t , τ represents the control torque at time t .

4. Experimental verification and case study

4.1. Experimental design and setup

Hardware Setup: In this study, a Franka Panda series 7-DoF robot is utilized. The robot's built-in force/torque sensor is employed to measure the contact forces experienced at the robot's end-effector during contact-based tasks. An end-effector device equipped with rollers is mounted at the robot's end-effector to simulate the execution tool in compliant and heterogeneous contact tasks.

Software System: The system runs on Ubuntu 20.04 LTS with the Noetic version, integrated with the Robot Operating System

¹ <https://web.casadi.org/>

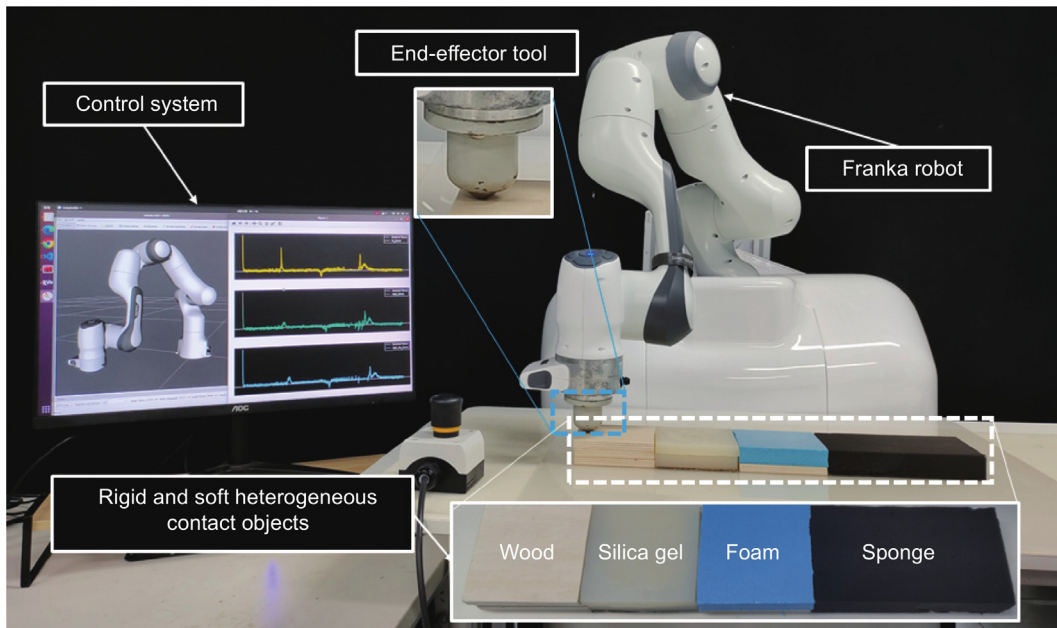


Fig. 4. Experimental setup.

Table 2
Illustration of the physical properties of four experimental materials.

Object	Material	E (MP)	ν	μ (μm)
Wood	Crosswise wood	5600	0.3	3.378
Foam	Polystyrene	3000	0.11	4.971
Silica gel	Silica gel	1200	0.48	2.783
Sponge	Polyurethane	840	0.34	9.329

(ROS) for data communication to achieve force-position coordinated optimization. The Franka Control Interface (FCI) Library² is utilized for robot data communication and control. The MPC optimizer provided by the CasADi library is invoked to conduct force-position coordinated optimization for the entire system.

Experimental Objects: Four materials with distinct stiffness characteristics are selected as experimental objects: wood board, foam board, silicone board, and sponge board. These materials represent different stiffness properties: rigid, weakly rigid, elastic, and soft. The specific parameters of the four materials are shown in Table 2.

Arrangement of contact objects along the Y-axis of the robot coordinate system: The contact objects are arranged sequentially along the Y-axis of the robot coordinate system as follows: wood board, silicone board, foam board, and sponge board. In medical and industrial applications such as ultrasound imaging, palpation, and processing/polishing of heterogeneous materials, operational continuity is essential. Among the four contact objects, the sponge board undergoes considerable deformation compared to the others. To ensure uninterrupted operation throughout the experiment, the sponge board is placed at the end of the sequence of contact objects. The experimental setup is illustrated in Fig. 4.

4.2. Theoretical verification and result analysis

4.2.1. Single-point contact task

This experiment predefined the contact positions for four contact objects to estimate their physical parameters. The objects are arranged in the order described earlier. The experiment consists of two phases: a non-contact phase and a physical parameter estimation phase.

During the non-contact phase, the robot end-effector slowly ascends to its maximum height along the z-axis to avoid contact with the contact objects, thus preventing interference with the estimation of physical parameters. Subsequently, it moves in the positive y-axis direction to reach the pre-defined contact positions. In the physical parameter estimation phase, the robot end-effector descends slowly until it contacts the contact objects, applying a constant force ($F_d = 10$ N). The objects are subjected to physical parameter estimation over a fixed duration ($t = 20$ s). The entire process of the fixed-point experiment and the estimated physical parameters for the four contact objects are illustrated in Fig. 5.

4.2.2. Continuous contact task

In the continuous contact experiment, four types of contact objects are positioned along the positive y-axis direction. Three different levels of desired force are set: $F_d = [5$ N, 10 N, 15 N]. At these varying desired force levels, two different control strategy methods are compared and validated against the method proposed in this paper.

- Method (i) enhances the existing force control by incorporating the Hertz contact model for kinematic modeling of contact, ensuring the stability of force along the z-axis. Impedance control is utilized for position control along the y-axis.
- Method (ii) employs a method based on dynamical linearization and Extended Kalman Filtering to predict contact position and stiffness. A variable impedance control strategy based on contact stiffness is used for position control of the robot, while traditional force control is applied for force along the z-axis.
- Method (iii) proposes a force-position coordinated control strategy based on MPC.

Four experiments are conducted for each method, focusing on recording changes in contact force along the z-axis, variations in z-axis contact position, and contact stiffness. A representative dataset from the experiments at the three different expected force levels is selected and presented graphically, as shown in Fig. 6.

² <https://frankaemika.github.io/libfranka/>

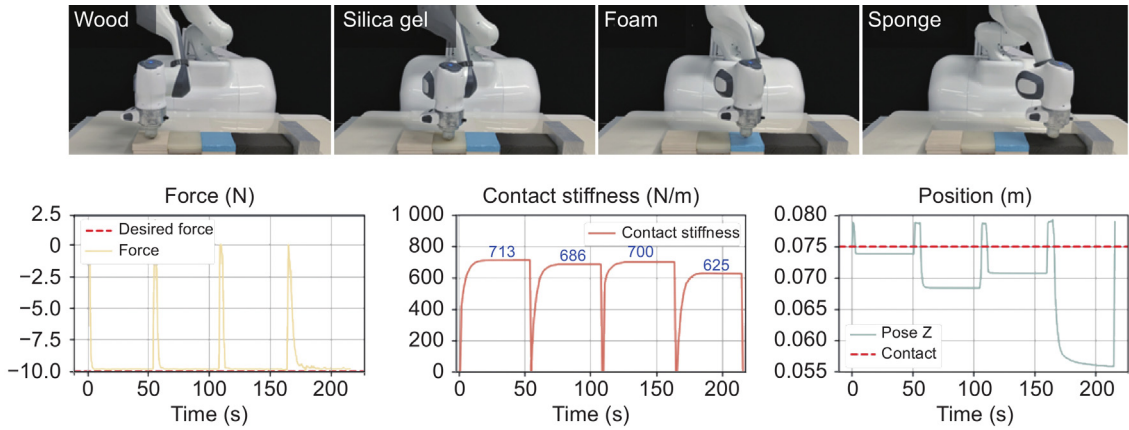


Fig. 5. The figure depicts the estimation results of the contact stiffness of the robot end-effector for four different contact objects. The top row of images shows real-world scenes illustrating the estimation of contact stiffness for the four different contact objects using the method proposed in this paper. The bottom row of images displays the contact force, contact stiffness, and contact Z-axis position during the estimation of contact stiffness. It can be seen that the magnitude of the contact stiffness of the four contact objects matches very well with their actual material mechanical properties and the material mechanical properties of the four contact objects are shown in Table 2.

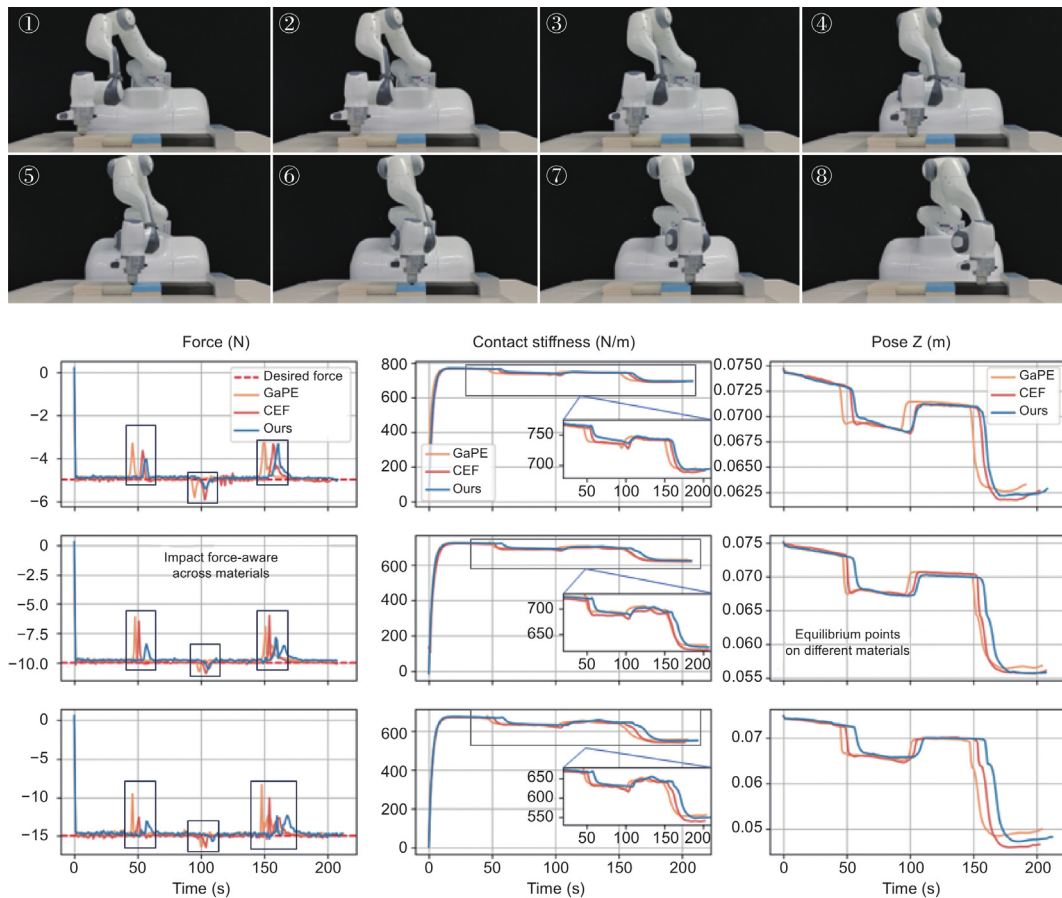


Fig. 6. Figure Legend: Contact Parameter Estimation + Force Control (GaPE), Contact Force Estimation + Position Control (CEF), Method proposed in this paper (Ours). The three rows of images represent numerical variations in contact force, contact stiffness, and contact position at different levels of expected force. During the process of the robot crossing different materials, significant fluctuations in contact force occur due to the discontinuous nature of the contact materials. Our method effectively limits the maximum fluctuations in contact force. The estimated contact stiffness by our proposed method remains stable and consistent with the material properties of the contact objects. Along the z-axis direction, the variation in contact position is also stable without significant fluctuations.

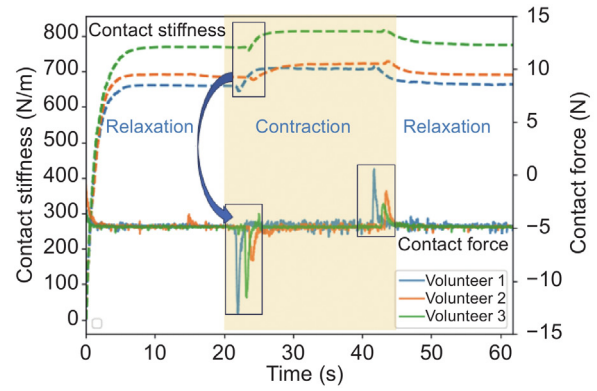
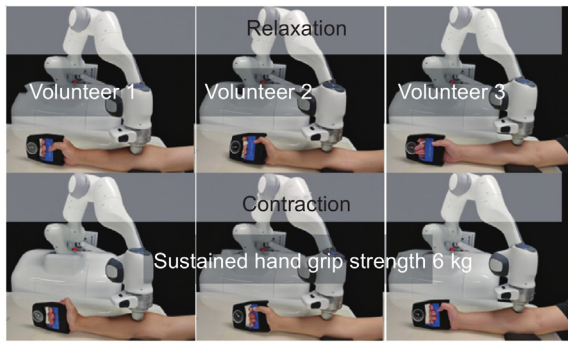


Fig. 7. The changes of forearm contact stiffness and contact force of three volunteers were analyzed. The white areas represented the relaxation phase of the volunteers' forearms, while the yellow areas represented the contraction phase of the forearm muscles. Three different colors represent the data of the three volunteers. In the image, the dotted line is the contact stiffness curve, and the solid line is the contact force curve. In the contraction phase, the contact stiffness changes obviously, but in the relaxation phase, the contact stiffness returns to stability. The fluctuations in contact force were attributed to temporary changes caused by the relaxation and contraction of the volunteers' forearm muscles. Throughout the process, the contact force remains relatively stable.

Table 3
Comparison of the force performance under various desired interactive forces across four experimental materials.

Sub.	Setup	F _{des} =5 N				F _{des} =15 N			
		Wood	Silica gel	Foam	Sponge	Wood	Silica gel	Foam	Sponge
S1	GaPE	4.87 ± 0.29	4.88 ± 0.29	4.91 ± 0.24	4.87 ± 0.38	14.67 ± 0.94	14.69 ± 0.83	14.75 ± 0.42	14.68 ± 0.80
	CFE	4.87 ± 0.34	4.85 ± 0.22	4.92 ± 0.20	4.97 ± 0.31	14.69 ± 0.99	14.65 ± 0.34	14.76 ± 0.34	14.67 ± 0.70
	Ours	4.96 ± 0.32	4.96 ± 0.29	4.99 ± 0.27	4.96 ± 0.34	14.96 ± 1.02	14.95 ± 0.53	15.03 ± 0.46	14.91 ± 0.78
S2	GaPE	4.87 ± 0.31	4.88 ± 0.25	4.91 ± 0.21	4.86 ± 0.33	14.68 ± 0.92	14.68 ± 0.59	14.74 ± 0.48	14.69 ± 0.80
	CFE	4.87 ± 0.30	4.87 ± 0.24	4.91 ± 0.21	4.87 ± 0.33	14.69 ± 0.92	14.66 ± 0.31	14.76 ± 0.30	14.67 ± 0.62
	Ours	4.97 ± 0.33	4.97 ± 0.30	5.00 ± 0.22	4.97 ± 0.34	14.97 ± 0.97	14.96 ± 0.45	15.01 ± 0.44	14.95 ± 0.82
S3	GaPE	4.88 ± 0.38	4.88 ± 0.28	4.93 ± 0.23	4.86 ± 0.35	14.70 ± 0.93	14.70 ± 0.44	14.75 ± 0.37	14.66 ± 0.80
	CFE	4.88 ± 0.35	4.87 ± 0.22	4.93 ± 0.19	4.85 ± 0.33	14.68 ± 0.89	14.66 ± 0.33	14.76 ± 0.38	14.68 ± 0.69
	Ours	4.97 ± 0.35	4.96 ± 0.31	5.01 ± 0.29	4.93 ± 0.37	14.96 ± 1.08	14.96 ± 0.46	15.02 ± 0.42	14.95 ± 0.73
S4	GaPE	4.88 ± 0.38	4.88 ± 0.31	4.93 ± 0.24	4.85 ± 0.36	14.70 ± 0.94	14.68 ± 0.63	14.76 ± 0.43	14.66 ± 0.80
	CFE	4.89 ± 0.40	4.87 ± 0.26	4.92 ± 0.19	4.86 ± 0.32	14.70 ± 0.94	14.66 ± 0.34	14.74 ± 0.36	14.66 ± 0.64
	Ours	4.97 ± 0.33	4.98 ± 0.29	5.00 ± 0.22	4.96 ± 0.33	14.97 ± 0.93	14.97 ± 0.54	15.02 ± 0.40	14.95 ± 0.87

To reflect the mechanical properties of the materials, the median of contact force ± standard deviation (SD) (where SD is obtained from Eq. (17)) is used. Table 3 presents the mechanical properties of four materials under three different expected force levels.

$$SD = \sqrt{\frac{1}{T} \sum_{t=1}^T (F_{cur} - F_{avg})^2} \quad (17)$$

Where, F_{cur} is the real-time measured force obtained by the robot's own force/torque sensor, F_{avg} is the average force of the sample data, and T is the number of samples.

From the experimental results, it is observed that due to the discontinuous nature of the contact objects, significant force fluctuations occur when the robot end effector moves across different materials. Across the three different levels of expected force experiments, the method proposed in this paper limits the maximum range of force fluctuations within 2 N, whereas the other two methods exhibit fluctuations around 4 N. Regarding the estimation of the physical parameters of the contact objects, the method proposed in this paper demonstrates better consistency compared to the other two methods. The robot end-effector maintains relative stability when moving along the z-axis, showing minimal observable fluctuations.

4.3. Case study on medical palpation

In the context of palpation in medical scenarios [46], doctors use controlled force to assess the texture, tenderness, or

anomalies of organs or tissues [47]. Traditional manual palpation tasks pose numerous challenges for surgeons, such as increased workload and infection risks. The method proposed in this study applies to medical palpation scenarios, aiming to mitigate these issues.

The experiment simulates the process of medical palpation. The robot end-effector applies a constant 5 N force to specific points on the surface tissue of a human volunteer, mimicking a doctor's palpation procedure. The experiment consists of two phases: relaxation and contraction. During the relaxation phase, the volunteer keeps their forearm relaxed. Under the robot's constant force pressing, the contact stiffness of the relaxed forearm is measured. In the contraction phase, the contraction level of the volunteer's forearm muscles is quantified using a grip strength meter, aiming for the volunteer to reach 6 kg of grip strength. With the forearm muscles contracted, the robot applies a constant force to measure the contact stiffness of the forearm in the contracted state. The volunteer maintains consistent relaxation and contraction durations of their forearm muscles throughout the experiment. The experimental results are depicted in Fig. 7.

In the experiment of localized pressing on the human forearm, it was observed that the stable stiffness values in the relaxed phase were consistent across objects due to similar skin conditions. In the contracted phase, as shown in the graph, noticeable changes in contact stiffness were evident due to muscle contraction. The method proposed in this study effectively reflects the stiffness of muscles and demonstrates that stiffness values return to stability upon relaxation.

Through this experiment, it is evident that the proposed method accurately estimates the contact stiffness of human skin

tissue post-palpation. Furthermore, it effectively portrays the varied mechanical characteristics of different objects, exhibiting continuity and stability.

5. Conclusion

This study introduces a model predictive control-based strategy for coordinated force-position optimization, validated through experiments involving compliant and heterogeneous contact tasks. The experiments include fixed-point and sliding-plane scenarios, aimed at evaluating the physical parameters of four contact objects. Additionally, the proposed method is applied to medical palpation and thin-walled component processing scenarios. The experimental outcomes highlight the considerable potential of the proposed optimization approach in tasks involving compliant and heterogeneous contacts within medical and industrial settings. The method proposed in this paper still has some shortcomings, during the contact task, the convergence speed of contact parameter estimation is relatively slow, which affects the overall operation time of the task. In the future, efforts should focus on improving the convergence speed of contact parameter estimation while ensuring its accuracy, thereby reducing the impact on the contact task.

CRedit authorship contribution statement

Haochen Zheng: Writing – original draft. **Xueqian Zhai:** Software. **Hongmin Wu:** Methodology. **Jia Pan:** Resources. **Zhihao Xu:** Conceptualization. **Xuefeng Zhou:** Supervision.

Declaration of competing interest

The authors declare that they have no known competing financial interests or personal relationships that could have appeared to influence the work reported in this paper.

Acknowledgments

This work was supported in part by the National Natural Science Foundation of China (62203126), the Science and Technology Plan Project of Guangdong Province (2023A0505010014), the Innovation and Technology Commission of the HKSAR Government under the InnoHK Initiative, and in part by the Key Areas R&D Program of Dongguan City (20201200300062), and the GDAS' Project of Science and Technology Development (2022GDA SZH-2022010108).

References

- [1] Mohammad Mir, Jiawen Chen, Aneri Patel, Meghan R. Pinezich, Brandon A. Guenthart, Gordana Vunjak-Novakovic, Jinho Kim, A minimally invasive robotic tissue palpation device, *IEEE Trans. Biomed. Eng.* (2024).
- [2] Qinghua Huang, Jiakang Zhou, Zhijun Li, Review of robot-assisted medical ultrasound imaging systems: Technology and clinical applications, *Neurocomputing* 559 (2023) 126790.
- [3] Yingxuan Zhang, Feng Ju, Xiaoyong Wei, Dan Wang, Yaoyao Wang, A piezoelectric tactile sensor for tissue stiffness detection with arbitrary contact angle, *Sensors* 20 (22) (2020) 6607.
- [4] Haochen Zheng, Xueqian Zhai, Shichao Gu, Zhaoyang Liao, Jia Pan, Zhihao Xu, Xuefeng Zhou, Shixin Mao, Hongmin Wu, Vision-based defects detection and interactive impedance control in robotic automated layup tasks, in: 2023 IEEE International Conference on Robotics and Biomimetics, ROBIO, 2023, pp. 1–6.
- [5] Matthias Mayr, Faseeh Ahmad, Konstantinos Chatzilygeroudis, Luigi Nardi, Volker Krueger, Skill-based multi-objective reinforcement learning of industrial robot tasks with planning and knowledge integration, in: 2022 IEEE International Conference on Robotics and Biomimetics, ROBIO, IEEE, 2022, pp. 1995–2002.
- [6] Cristian Camilo Beltran-Hernandez, Damien Petit, Ixchel Georgina Ramirez-Alpizar, Takayuki Nishi, Shinichi Kikuchi, Takamitsu Matsubara, Kensuke Harada, Learning force control for contact-rich manipulation tasks with rigid position-controlled robots, *IEEE Robot. Autom. Lett.* 5 (4) (2020) 5709–5716.
- [7] Chao Zeng, Chenguang Yang, Zehao Jin, Jianwei Zhang, Hierarchical impedance, force, and manipulability control for robot learning of skills, *IEEE/ASME Trans. Mechatronics* (2024).
- [8] Sotaro Katayama, Toshiyuki Ohtsuka, Whole-body model predictive control with rigid contacts via online switching time optimization, in: 2022 IEEE/RSJ International Conference on Intelligent Robots and Systems, IROS, 2022, pp. 8858–8865.
- [9] Kaidong Liu, Bin Xie, Zhouyang Chen, Zhenhao Luo, Shan Jiang, Zhen Gao, Human-robot skill transferring and inverse velocity admittance control for soft tissue cutting tasks, *Agriculture* 14 (3) (2024) 394.
- [10] Jing Luo, Chaoyi Zhang, Weiyong Si, Yiming Jiang, Chenguang Yang, Chao Zeng, A physical human-robot interaction framework for trajectory adaptation based on human motion prediction and adaptive impedance control, *IEEE Trans. Autom. Sci. Eng.* (2024).
- [11] Basem Adel Aly, Tobias Low, Derek Long, Peter Brett, Craig Baillie, Tactile sensing for tissue discrimination in robotic meat cutting: A feasibility study, *J. Food Eng.* 363 (2024) 111754.
- [12] Tobias Gold, Andreas Völz, Knut Graichen, Model predictive interaction control for robotic manipulation tasks, *IEEE Trans. Robot.* 39 (1) (2023) 76–89.
- [13] Tobias Gold, Andreas Völz, Knut Graichen, Model predictive position and force trajectory tracking control for robot-environment interaction, in: 2020 IEEE/RSJ International Conference on Intelligent Robots and Systems, IROS, 2020, pp. 7397–7402.
- [14] Junjie Shen, Dennis Hong, Optimal linearization via quadratic programming, *IEEE Robot. Autom. Lett.* 5 (3) (2020) 4572–4579.
- [15] Zhihong Jiang, Weigang Zhou, Hui Li, Yang Mo, Wencheng Ni, Qiang Huang, A new kind of accurate calibration method for robotic kinematic parameters based on the extended Kalman and particle filter algorithm, *IEEE Trans. Ind. Electron.* 65 (4) (2017) 3337–3345.
- [16] Tobias Gold, Andreas Völz, Knut Graichen, Model predictive position and force trajectory tracking control for robot-environment interaction, in: 2020 IEEE/RSJ International Conference on Intelligent Robots and Systems, IROS, 2020, pp. 7397–7402.
- [17] Mohamed Elobaid, Giulio Romualdi, Gabriele Nava, Lorenzo Rapetti, Hosameldin Awadalla Omer Mohamed, Daniele Pucci, Online non-linear centrodial MPC for humanoid robots payload carrying with contact-stable force parametrization, in: 2023 IEEE International Conference on Robotics and Automation, ICRA, 2023, pp. 12233–12239.
- [18] Guillaume Bellegarda, Katie Byl, An online training method for augmenting MPC with deep reinforcement learning, in: 2020 IEEE/RSJ International Conference on Intelligent Robots and Systems, IROS, 2020, pp. 5453–5459.
- [19] Yuquan Wang, Niels Dehio, Abderrahmane Kheddar, On inverse inertia matrix and contact-force model for robotic manipulators at normal impacts, *IEEE Robot. Autom. Lett.* 7 (2) (2022) 3648–3655.
- [20] Fugui Xie, Zenghui Chong, Xin-Jun Liu, Huichan Zhao, Jinsong Wang, Precise and smooth contact force control for a hybrid mobile robot used in polishing, *Robot. Comput.-Integr. Manuf.* 83 (2023) 102573.
- [21] Alp Aydinoglu, Victor M. Preciado, Michael Posa, Contact-aware controller design for complementarity systems, in: 2020 IEEE International Conference on Robotics and Automation, ICRA, 2020, pp. 1525–1531.
- [22] Mohsen Sombolstan, Quan Nguyen, Hierarchical adaptive control for collaborative manipulation of a rigid object by quadrupedal robots, in: 2023 IEEE/RSJ International Conference on Intelligent Robots and Systems, IROS, 2023, pp. 2752–2759.
- [23] Sébastien Kleff, Justin Carpentier, Nicolas Mansard, Ludovic Righetti, On the derivation of the contact dynamics in arbitrary frames: Application to polishing with talos, in: 2022 IEEE-RAS 21st International Conference on Humanoid Robots (Humanoids), 2022, pp. 512–517.
- [24] Zehao Jin, Dongdong Qin, Andong Liu, Wen-an Zhang, Li Yu, Model predictive variable impedance control of manipulators for adaptive precision-compliance tradeoff, *IEEE/ASME Trans. Mechatronics* 28 (2) (2023) 1174–1186.
- [25] Miroslav Bogdanovic, Majid Khadiv, Ludovic Righetti, Learning variable impedance control for contact sensitive tasks, *IEEE Robot. Autom. Lett.* 5 (4) (2020) 6129–6136.
- [26] Zhu Dachang, Du Baolin, Zhu Puchen, Chen Shouyan, Constant force PID control for robotic manipulator based on fuzzy neural network algorithm, *Complexity* 2020 (1) (2020) 3491845.
- [27] Saif Sidhik, Mohan Sridharan, Dirk Ruiken, Towards an online framework for changing-contact robot manipulation tasks, in: 2021 IEEE/RSJ International Conference on Intelligent Robots and Systems, IROS, 2021, pp. 5203–5210.
- [28] Ning Wang, Chuize Chen, Alessandro Di Nuovo, A framework of hybrid force/motion skills learning for robots, *IEEE Trans. Cogn. Dev. Syst.* 13 (1) (2021) 162–170.

- [29] Huanyu Tian, Zhe Han, Yang Wang, Xiaolong Zhu, Weijun Zhang, Zhengjie Wang, Changsheng Li, Xingguang Duan, Virtual-fixture based osteotomy shared control: A framework for human-robot shared surgical osteotomy manipulation, *IEEE Trans. Med. Robotics Bionics* (2023).
- [30] Emanuele Magrini, Alessandro De Luca, Hybrid force/velocity control for physical human-robot collaboration tasks, in: 2016 IEEE/RSJ International Conference on Intelligent Robots and Systems, IROS, 2016, pp. 857–863.
- [31] Junling Fu, Ilaria Burzo, Elisa Iovene, Jianzhuang Zhao, Giancarlo Ferrigno, Elena De Momi, Optimization-based variable impedance control of robotic manipulator for medical contact tasks, *IEEE Trans. Instrum. Meas.* 73 (2024) 1–8.
- [32] Yanan Li, Gowrishankar Ganesh, Nathanaël Jarrassé, Sami Haddadin, Alin Albu-Schaeffer, Etienne Burdet, Force, impedance, and trajectory learning for contact tooling and haptic identification, *IEEE Trans. Robot.* 34 (5) (2018) 1170–1182.
- [33] Yang Li, Wenjie Lin, Zhehao Jin, Xiang Wu, Qun Lu, Hui Dong, Sensor-free variable impedance control using quadratic programming and extended state observer, in: 2024 IEEE International Conference on Industrial Technology, ICIT, 2024, pp. 1–5.
- [34] Xing Liu, Panfeng Huang, Zhengxiong Liu, A novel contact state estimation method for robot manipulation skill learning via environment dynamics and constraints modeling, *IEEE Trans. Autom. Sci. Eng.* 19 (4) (2022) 3903–3913.
- [35] Rui Wu, Aude Billard, Learning from demonstration and interactive control of variable-impedance to cut soft tissues, *IEEE/ASME Trans. Mechatronics* 27 (5) (2022) 2740–2751.
- [36] Haohui Huang, Chenguang Yang, C.L. Philip Chen, Optimal robot–environment interaction under broad fuzzy neural adaptive control, *IEEE Trans. Cybern.* 51 (7) (2021) 3824–3835.
- [37] Mohammad Hossein Hamedani, Hamid Sadeghian, Maryam Zekri, Farid Sheikholeslam, Mehdi Keshmiri, Intelligent impedance control using wavelet neural network for dynamic contact force tracking in unknown varying environments, *Control Eng. Pract.* 113 (2021) 104840.
- [38] Tao Pang, Russ Tedrake, A convex quasistatic time-stepping scheme for rigid multibody systems with contact and friction, in: 2021 IEEE International Conference on Robotics and Automation, ICRA, 2021, pp. 6614–6620.
- [39] Joonhee Jo, Gyunghoon Park, Yonghwan Oh, Robust walking stabilization strategy of humanoid robots on uneven terrain via QP-based impedance/admittance control, *Robot. Auton. Syst.* 154 (2022) 104148.
- [40] Jinda Cui, Jiawei Xu, David Saldana, Jeff Trinkle, Toward fine contact interactions: Learning to control normal contact force with limited information, in: 2023 IEEE International Conference on Robotics and Automation, ICRA, 2023, pp. 3926–3932.
- [41] Jian Li, Yisheng Guan, Haowen Chen, Bing Wang, Tao Zhang, Robotic polishing of unknown-model workpieces with constant normal contact force control, *IEEE/ASME Trans. Mechatronics* 28 (2) (2023) 1093–1103.
- [42] Ross Hartley, Maani Ghaffari, Ryan M. Eustice, Jessy W Grizzle, Contact-aided invariant extended Kalman filtering for robot state estimation, *Int. J. Robot. Res.* 39 (4) (2020) 402–430.
- [43] Jinjun Duan, Yahui Gan, Ming Chen, Xianzhong Dai, Adaptive variable impedance control for dynamic contact force tracking in uncertain environment, *Robot. Auton. Syst.* 102 (2018) 54–65.
- [44] Francisco Rubio, Francisco Valero, Carlos Llopis-Albert, A review of mobile robots: Concepts, methods, theoretical framework, and applications, *Int. J. Adv. Robot. Syst.* 16 (2) (2019) 1729881419839596.
- [45] Said Zahmoun, Ahmed Ouammi, Roberto Sacile, Rachid Benchrifa, Enrico Zero, Optimal operation scheduling of a combined wind-hydro system for peak load shaving, *IEEE Trans. Autom. Sci. Eng.* (2023) 1–14.
- [46] Giovanni Faoro, Sabina Maglio, Stefano Pane, Veronica Iacovacci, Arianna Menciassi, An artificial intelligence-aided robotic platform for ultrasound-guided transcarotid revascularization, *IEEE Robot. Autom. Lett.* 8 (4) (2023) 2349–2356.
- [47] Davide Doria, Simone Fani, Andrea Giannini, Tommaso Simoncini, Matteo Bianchi, Enhancing the localization of uterine leiomyomas through cutaneous softness rendering for robot-assisted surgical palpation applications, *IEEE Trans. Haptics* 14 (3) (2021) 503–512.